Impact of asymmetries on fuel performance in inertial confinement fusion

M. Gatu Johnson, B. D. Appelbe, J. P. Chittenden, J. Delettrez, C. Forrest, J. A. Frenje, V. Yu. Glebov, W. Grimble, B. M. Haines, I. Igumenshchev, R. Janezic, J. P. Knauer, B. Lahmann, F. J. Marshall, T. Michel, F. H. Séguin, C. Stoeckl, C. Walsh, A. B. Zylstra, and R. D. Petrasso

Phys. Rev. E **98**, 051201 — Published 5 November 2018

DOI: 10.1103/PhysRevE.98.051201

Impact of asymmetries on fuel performance in Inertial Confinement Fusion

M. Gatu Johnson[1], B.D. Appelbe,[2] J.P. Chittenden,[2] J. Delettrez,[3] C. Forrest,[3] J.A. Frenje,[1] V.Yu. Glebov,[3] W. Grimble,[3] B.M. Haines,[4] I. Igumenshchev,[3] R. Janezic,[3] J.P. Knauer,[3] B. Lahmann,[1] F. Marshall,[3] T. Michel,[3] F.H. Séguin,[1] C. Stoeckl,[3] C. Walsh,[2] A.B. Zylstra,[4] R.D. Petrasso[1]

[1]Massachusetts Institute of Technology Plasma Science and Fusion Center, Cambridge, MA 02139, USA
[2]Centre for Inertial Fusion Studies, The Blackett Laboratory, Imperial College, London SW7 2AZ, United Kingdom
[3]Laboratory for Laser Energetics, University of Rochester, Rochester, NY 14623, USA
[4]Los Alamos National Laboratory, Los Alamos, NM 87545, USA

Low-mode asymmetries prevent effective compression, confinement and heating of the fuel in inertial confinement fusion (ICF) implosions and their control is essential to achieving ignition. Ion temperatures (T_{ion}) in ICF experiments are inferred from the broadening of primary neutron spectra. Directional motion (flow) of the fuel at burn also impacts broadening and will lead to artificially inflated "T_{ion}" values. Flow due to low-mode asymmetries is expected to give rise to line-of-sight variations in measured T_{ion}. We report on intentionally asymmetrically driven experiments at the OMEGA laser facility designed to test the ability to accurately predict and measure line-of-sight differences in apparent T_{ion} due to low-mode asymmetry-seeded flows. Contrasted to Chimera and xRAGE simulations, the measurements demonstrate how all asymmetry seeds have to be considered to fully capture the flow field in an implosion. In particular, flow induced by the stalk that holds the target is found to interfere with the seeded asymmetry. A substantial stalk-seeded asymmetry in the areal density of the implosion is also observed.

Inertial confinement fusion (ICF) aims to achieve fusion burn by symmetrically compressing a spherical capsule filled with deuterium-tritium (DT) fuel to high convergence using lasers, either indirectly using a hohlraum [1] or with the laser beams directly incident on the target [2]. Independent of approach, control of low-mode asymmetries is of vital importance in the quest for ICF ignition [3-5]; such low-mode asymmetries have been identified as a primary performance-limiting factor for integrated NIF experiments [6]. Low-mode asymmetries will prevent effective compression and confinement of the fuel as well as effective conversion of shell kinetic energy to thermal energy of the fuel [7-9]. A consequence of low-mode asymmetries is residual kinetic energy of the fuel at burn (see e.g. [3,6]). Accurate understanding of plasma ion temperature (T_{ion}) from ICF implosions is important as T_{ion} is used as input for calculation of the pressure performance metric used to gauge progress towards ignition [10-12]. T_{ion} is traditionally inferred from the broadening of neutron spectra [13] and will thus also be sensitive to any residual fuel flows at burn, which will serve to artificially inflate the measured "T_{ion}" [14-16] and, if the flows are asymmetric, lead to line-of-sight (LOS) variations in observed T_{ion}. Such flow broadening has been invoked to explain discrepancies between measured and simulated T_{ion} for both indirect [17] and direct [18] drive implosions, but outstanding problems remain. As an example, minimal T_{ion} LOS variations have been observed in indirectly driven implosions at the NIF, while a large difference in measured DD and DT T_{ion} indicates the presence of residual flows in these experiments [17]. In contrast, large T_{ion} LOS variations have been observed for directly driven implosions at OMEGA [18]. An improved understanding of the flow field in ICF implosions is essential both for assessing the impact of and learning how to mitigate low-mode asymmetries, and for interpretation of T_{ion} measurements.

In this paper, we report on results from an experiment at the OMEGA laser facility [19] with intentionally imposed mode 2 asymmetries. The purpose of this experiment was to test the capability to accurately predict and measure the impact of a pre-imposed low-mode asymmetry on measured DT neutron spectra. Comparing T_{ion} asymmetry measurements from these perturbed implosions with 3D simulations [20] not including the capsule stalk mount, we find that while the simulations partly capture the measurements, there is a clear remaining discrepancy. These T_{ion} asymmetry results in combination with x-ray self-emission imaging and measurements of areal density (ρR) asymmetries lead to the conclusion that the differences between measurements and simulations arise to due interplay between a stalk-seeded low-mode asymmetry and the imposed mode 2.

In the OMEGA experiment, five DT^{3}He-gas-filled, 870-μm outer diameter plastic capsules with 14.5-μm-thick shells were imploded with all 60 available OMEGA laser beams [21]. A 1-ns duration laser pulse was used, with distributed phase plates and with two-dimensional smoothing by spectral dispersion [22] and polarization smoothing [23] applied. Total on-target illumination non-uniformity related to these factors <2% rms [24]. Each capsule was held at the target chamber center (TCC) using a 17-μm diameter SiC stalk attached with a glue spot (FIG. 1a). One capsule was symmetrically imploded for reference with nominally 0.45 kJ laser energy per beam. Two mode 2 drive asymmetries with the same magnitude (19% peak-to-valley) but different orientation were designed for the remaining implosions by reducing the laser beam energy for 20-24 selected beams in two opposing cones around the implosion. These two asymmetries, henceforth denoted Asym. A (Fig. 1b) and Asym. B (Fig. 1c), were oriented to maximize the expected signatures in the three primary neutron spectrometer LOS (identified with black plus signs in Fig. 1b,c), and to "flip" the asymmetry between the two orientations. Two implosions of each asymmetry type were executed. The neutron spectra were measured using three neutron time-of-flight (nTOF) detectors: a scintillator-based detector 12m from the implosion (12mntof), a scintillator-based detector 15.8m from the implosion (15.8mntof) and a CVD-diamond based detector 5m from the implosion (5.0mcvd) [26]. Implosion performance parameters are summarized in the supplemental material [27]. Measured T_{ion} ranged from 5.5-6.5 keV (including all LOS on all implosions). A DT neutron yield of 1.2×10^{13} was observed for the symmetric implosion, while an average yield of 7.4×10^{12} was obtained from the asymmetric implosions. This observed 36% yield reduction compares reasonably well to a 46% average reduction expected

from 3D simulations. We note that the detrimental impact of low-mode asymmetries is expected to increase with implosion convergence [12], which explains why the yield reduction is not higher for these relatively low-convergence implosions.

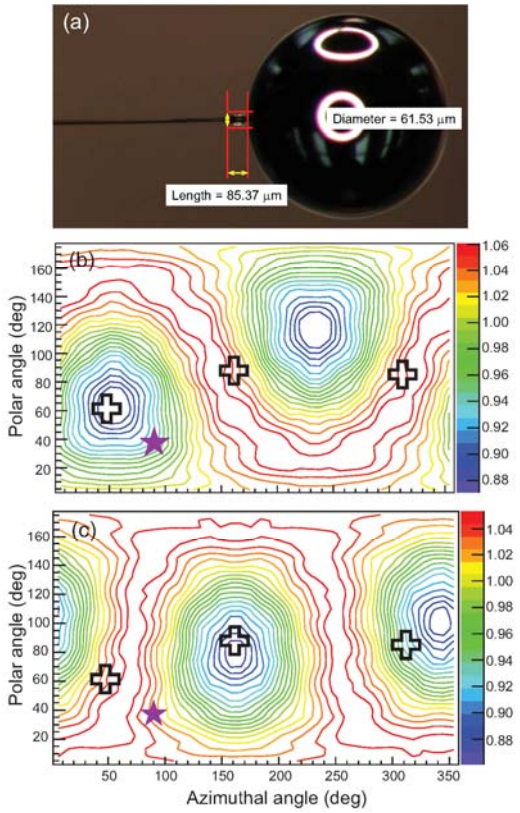

FIG 1: (a) Picture of CH-shell capsule used in the OMEGA experiment mounted to the stalk with a glue spot with characterized length and diameter. (b) Asymmetry A and (c) Asymmetry B contour maps of laser intensity as a function of polar and azimuthal angle relative to the average laser intensity, illustrating the imposed mode 2. The plus signs represent the locations of the primary nTOF detectors, from left to right 15.8mntof, 12mntof and 5mcvd. The purple star represents the location of the stalk.

The implosions were simulated post-shot using the 3D Chimera code [20]. Chimera is initialized after the end of the laser pulse using output from 1D HYADES [28] simulations, and run through convergence and disassembly. Previous work has shown that low-mode asymmetries can be expected to arise due to engineering features such as the stalk mount, fill tube and/or support tent used to hold and fill an ICF target [29-33], due to unintended laser drive asymmetries [9,34-35], or due to unintentional capsule misalignment (offset) [36]. Capsule offsets are small for these room temperature implosions [37,38]. The Chimera simulations, which use multi-group radiation transport, implement the measured laser beam energy balance [39-40] and are hence expected to capture effects due to laser drive asymmetry (this is done by initializing different regions around the implosion with HYADES simulations with varying drive). However, the simulations do not include the stalk mount. Synthetic neutron spectra are calculated for the three nTOF LOS [41] and simulated T_{ion} inferred from fits to the synthetic spectra.

Each nTOF provides a single neutron spectrum measurement integrated over burn, which means that the inferred T_{ion} is impacted by a burn-weighted averaging of the flow. The expected sign of the T_{ion} asymmetry depends sensitively on the timing of outflow along the asymmetry axis relative to burn. Early in the implosion, when the capsule is still compressing along all axes, maximum instantaneous T_{ion} is expected perpendicular to the asymmetry, while later in the implosion, after outflow starts along the axis of reduced laser energy, maximum T_{ion} is expected parallel to the asymmetry. According to the Chimera simulation, peak neutron production happens after the fuel has started moving outwards along the axis of the imposed mode 2 but while it is still moving inwards perpendicular to the asymmetry, which leads to maximum observed T_{ion} parallel to the asymmetry.

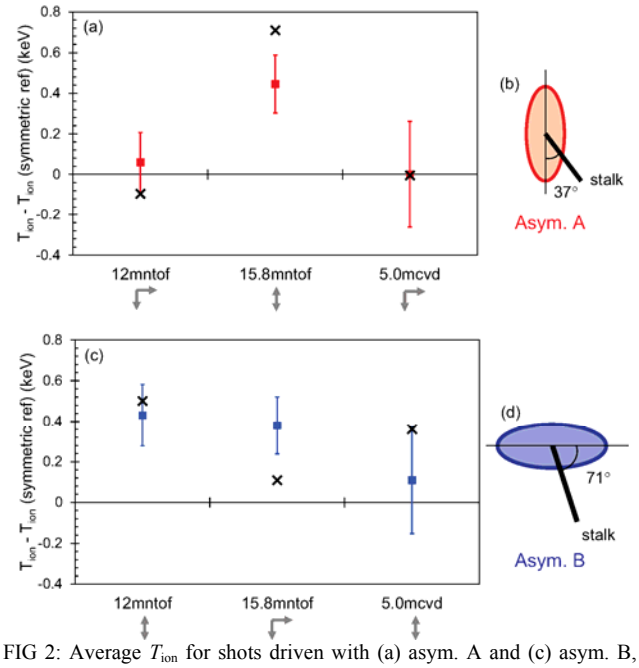

FIG 2: Average T_{ion} for shots driven with (a) asym. A and (c) asym. B, minus T_{ion} for the symmetric reference shot. Points with error bars represent measured values in the three lines-of-sight using the 12mntof, 15.8mntof and 5.0mcvd detectors, black crosses 3D Chimera-simulated values for the same lines-of-sight. The gray arrows below the plots indicate whether a detector is located parallel or perpendicular to the axis of the imposed mode 2 asymmetry. Also shown are cartoons illustrating the angle between the imposed mode 2 and the stalk for the two drive configurations, asym. A in (b) and asym. B in (d); the thin black line represents the asymmetry axis.

Measured and Chimera-simulated T_{ion} for the three nTOF LOS are contrasted in Fig. 2. Panel (a) shows the average difference in T_{ion} for each LOS between the symmetric reference and the two Asym. A implosions, panel (c) shows the same quantity for the two Asym. B implosions. (The symmetric reference is subtracted out to correct for any systematic differences between the three nTOF detectors.) The arrows below the plots indicate whether a detector is located parallel or perpendicular to the axis of the imposed mode 2 asymmetry. For Asym. A (Fig. 2a), a clear enhancement in measured T_{ion} relative to the reference implosion is observed parallel to the imposed mode 2 (15.8mntof), as expected from the Chimera simulations

albeit slightly weaker than simulated. For Asym. B (Fig. 2c), the Chimera simulations also predict enhanced T_{ion} relative to the symmetric reference parallel to the imposed mode 2. In contrast, experimentally an overall enhancement in T_{ion} is observed in this case. The observed differences between measured and simulated results are believed to arise due to interplay between the imposed mode 2 and flow seeded by the capsule stalk mount, which is not included in the simulations. For Asym. A, the mode 2 is imposed at an angle of 37° from the stalk that holds the capsule (Fig. 2b; in this illustration, the laser power is reduced at the tips of the ellipse and the thin black line represents the mode 2 axis). We conjecture that the experimental effect on T_{ion} is smaller than simulated due to interference of stalk-seeded flow, which is not included in the simulation. For Asym. B, the mode 2 is imposed at a much larger angle to the stalk of 71° (Fig. 2d). In this case, it appears as though the flows seeded by the mode 2 and the stalk counteract each other to eliminate LOS variations, while there is still clearly a substantial flow field induced in the implosion.

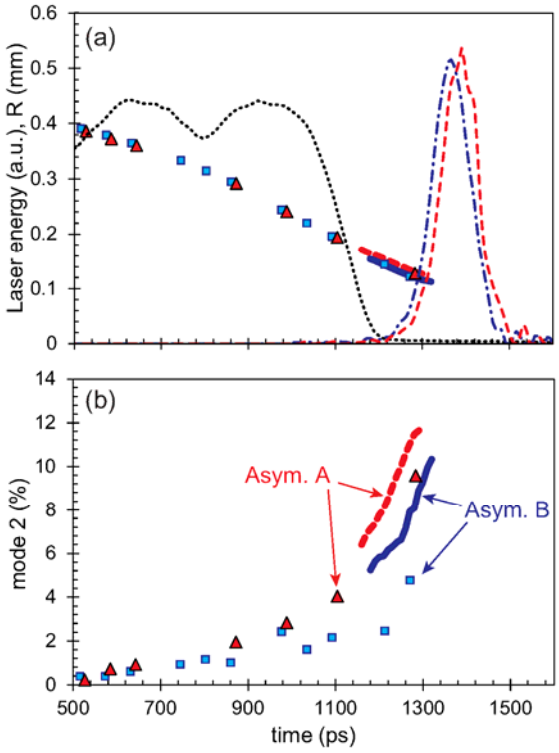

FIG 3: (a) Measured shell trajectories as inferred from self-emission x-ray images for asym. A (red triangles) and asym. B (blue squares), contrasted to shell trajectories as inferred from Chimera-simulated x-ray images (thick red dashed and solid blue lines for the two cases). Also shown is the laser pulse shape (dotted black) and the burn history for the two implosions (red dashed line for asym. A, broken blue line for asym. B). (b) Mode 2 amplitude inferred from measured and simulated x-ray images, with the same color coding as in (a).

The hypothesis of asymmetry seed interplay is further supported by self-emission x-ray imaging of the converging implosions using an x-ray framing camera fielded at 79° from the imposed Asym. A and at 42° from the imposed Asym. B. Shell radius and mode 2 as a function of time inferred from the measured x-ray images [42] are contrasted to Chimera simulations in Fig. 3. Because of the different fielding angle relative to the imposed mode 2, the x-ray images will see 98% of the asymmetry for Asym. A and 61% for Asym. B. (As the simulations consider the physical location of the x-ray framing camera, this is true both for experiments and simulation.) The implosion trajectory (radius vs time) is extremely well captured in the post-shot simulations for both Asym. A and B (Fig. 3a), demonstrating that the simulations describe the overall implosion dynamics very well (note that simulated trajectories are only available at late time because of how Chimera is initialized). In contrast, the observed mode 2 (Fig. 3b) is significantly better captured for the Asym. A than for the Asym. B case. This again is consistent with an effect not included in the simulation (the stalk) substantially interfering with the imposed mode 2 for the Asym. B scenario.

Areal density asymmetry measurements for these implosions provide further evidence of the impact of the stalk. The experiment used a capsule fill gas composed of 38% D, 38% T and 24% ^{3}He, with ^{3}He included to allow for directional measurements of the D^{3}He proton spectrum. LOS variations in areal density were inferred based on D^{3}He-proton energy downshifts observed using five different proton spectrometers distributed around the implosion [43,44]. The results for the symmetric reference implosion are contrasted to 2D xRAGE simulations [30,45] in Fig. 4. The xRAGE simulations include the stalk, but cannot simultaneously capture impact of stalk and the imposed mode 2 because of the 2D geometry. (This is why they are compared only to measurements from the symmetric reference implosion.) We find that while the average measured ρR (points with error bars in Fig. 4) is significantly higher than predicted by xRAGE (solid curve), the shape of the observed areal density variation is well captured by the simulation. If the amplitude of the xRAGE-simulated ρR curve is increased a factor 1.44, an excellent description of the data is obtained (dashed curve; χ^2_{red}=0.5). For comparison, fitting a straight line (ρR=34.6 mg/cm^2) to the data provides a much worse description (broken curve, χ^2_{red}=1.6). The data provide evidence that the weak spot in ρR around the stalk predicted by xRAGE is a real effect. We additionally note that while the implosions with imposed mode 2 show more variations in inferred ρR around the implosion than the symmetric reference as expected, all demonstrate the same weak spot at the location closest to the stalk [44].

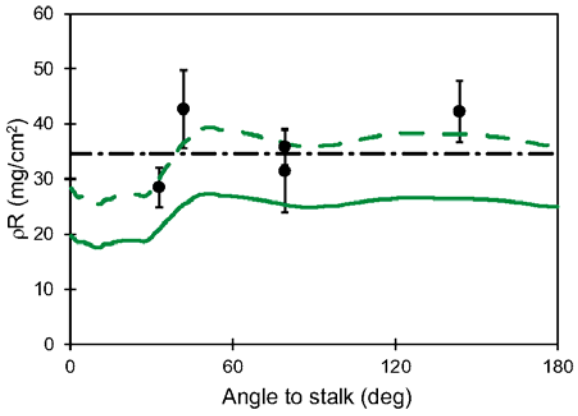

FIG 4: Measured (points with error bars) and 2D-xRAGE-simulated (solid green line) ρR for the symmetric reference shot as a function of angle to the stalk. While the xRAGE simulation underestimates the

overall ρR magnitude, it captures the shape of the asymmetry remarkably well: the dashed green line representing the xRAGE simulation renormalized to match the amplitude of the data matches the measurement with χ^2_{red}=0.5. In contrast, using a flat ρR (broken black curve) to describe the data gives χ^2_{red}=1.6.

In summary, T_{ion} asymmetry measurements and x-ray self-emission imaging contrasted to 3D Chimera simulations both indicate a missing piece in the simulation, which based on the setup geometry is most likely flow induced by the stalk holding the capsule. ρR asymmetry measurements compared to 2D xRAGE simulations also indicate that the stalk introduces a substantial "weak spot" in the implosion, expected to be accompanied by an induced flow in the fuel. Together these observations lead to the conclusion that counteracting flows due to different asymmetry seeds must be considered when interpreting results from ICF implosions. When the various asymmetries directly counteract each other, as in Asym. B, an overall enhancement but small LOS variations in T_{ion} are observed. On the other hand, if asymmetry seeds align to reinforce each other, we can expect more significant LOS variations in T_{ion}. This type of argument likely explains the differences between T_{ion} observations for OMEGA and NIF cryogenically layered implosions discussed in the introduction. At the NIF, we expect at minimum a mode 2 asymmetry in the drive due to the hohlraum geometry [34-35], a mode 4 asymmetry seeded by the capsule support tent [32-33,46], and a mode 1 asymmetry seeded by the fill tube [33]. Based on the results presented in this paper, we hypothesize that the complex interactions of these modes lead to low LOS variations in T_{ion} but large overall flow broadening of the neutron spectra, consistent with NIF observations [17]. At OMEGA, on the other hand, we expect a mode 1 drive asymmetry [9], mode 1 introduced by unintentional capsule offsets [7], and mode 1 from the stalk; based on the present work, for shots where these various asymmetries align, we expect them to reinforce each other leading to large LOS variations in T_{ion}.

A couple of interesting additional observations can be made based on the present work. First, while there is no way of separating thermal from flow contributions to observed T_{ion} in the measurement, this is straightforward in the simulations. According to the Chimera simulations [47], the minimum observed T_{ion} is 0.35 keV higher than thermal "no-flow" T_{ion} for the symmetric implosion, and 0.69-0.82 keV higher than no-flow T_{ion} for each of the asymmetrically driven implosions. This means that taking the minimum measured T_{ion} as a representation of thermal T_{ion} when calculating the pressure, as is currently often done for lack of a better method [12,48], is likely to significantly miss the mark. Second, the observed ρR asymmetry is an interesting result on its own. With an asymmetry this significant observed even for these relatively low-convergence implosions, significantly larger stalk-seeded ρR asymmetries can be expected to develop when the implosion is driven to converge more. Interestingly, recent efforts to predict performance of cryogenically layered implosions on OMEGA using data-driven statistical modeling suggest the presence of a persistent, systematic but as of yet unidentified asymmetry seed in these implosions [49]; our results point to the target mount as the likely culprit.

Ultimately, a full understanding of the flow field in implosions and the impact of different asymmetry seeds is important in the efforts to control and minimize the imposed asymmetries, or maybe even exploit the flow field, as proposed in Ref. [50]. The results described in this paper lay the groundwork for understanding the flow field in terms of asymmetry seed interplay, motivating further simulations and experiments to gain a broader understanding of the relationships.

In conclusion, T_{ion} and ρR asymmetry measurements and x-ray self-emission imaging from an experiment with imposed mode 2 asymmetries contrasted to simulations demonstrate the impact of asymmetry seed interplay on the flow field in ICF implosions, and the impact of the capsule stalk mount on ρR asymmetries. The results represent a major step forward in the understanding of asymmetry seed impact on implosion dynamics, which is a complex problem that must be mastered to achieve ICF ignition.

The authors sincerely thank the OMEGA operations staff who supported this work, Bob Frankel and Ernie Doeg for processing the CR-39, and Michelle Evans for characterizing the target glue spots. This material is based upon work supported by the Department of Energy, National Nuclear Security Administration under Award Number DE-NA0002949, by the National Laser Users' Facility under award number DE-NA0002726, by LLE under award number 415935-G, and by Los Alamos National Laboratory operated by Los Alamos National Security, LLC for the U.S. Department of Energy NNSA under Contract No. DE-AC52-06NA25396. This report was prepared as an account of work sponsored by an agency of the United States Government. Neither the United States Government nor any agency thereof, nor any of their employees, makes any warranty, express or implied, or assumes any legal liability or responsibility for the accuracy, completeness, or usefulness of any information, apparatus, product, or process disclosed, or represents that its use would not infringe privately owned rights. Reference herein to any specific commercial product, process, or service by trade name, trademark, manufacturer, or otherwise does not necessarily constitute or imply its endorsement, recommendation, or favoring by the United States Government or any agency thereof. The views and opinions of authors expressed herein do not necessarily state or reflect those of the United States Government or any agency thereof.

References

1. J.D. Lindl, P. Amendt, R.L. Berger, S.G. Glendinning, S.H. Glenzer, S.W. Haan, R.L. Kauffman, O.L. Landen and L.J. Suter, Phys. Plasmas **11**, 339 (2004).
2. R.S. Craxton et al., Phys. Plasmas **22**, 110501 (2015).
3. B. K. Spears, M.J. Edwards, S. Hatchett, J. Kilkenny, J. Knauer, A. Kritcher, J. Lindl, D. Munro, P. Patel, H.F. Robey and R.P.J. Town, Phys. Plasmas **21**, 042702 (2014).
4. C. Cerjan, P.T. Springer, and S.M. Sepke, Phys. Plasmas **20**, 056319 (2013).
5. A.L. Kritcher et al., Phys. Plasmas **21**, 042708 (2014).
6. A.L. Kritcher et al., Phys. Plasmas **23**, 052709 (2016).
7. I.V. Igumenshchev et al., Phys. Plasmas **23**, 052702 (2016).
8. I.V. Igumenshchev, Phys. Plasmas **24**, 056307 (2017).
9. R.C. Shah et al., Phys. Rev. Lett. **118**, 135001 (2017).
10. R. Betti, P.Y. Chang, B. K. Spears, K.S. Anderson, J. Edwards, M. Fatenejad, J.D. Lindl, R.L. McCrory, R. Nora and D. Shvarts, Phys. Plasmas **17**, 058102 (2010).
11. R. Betti, A.R. Christopherson, B.K. Spears, R. Nora, A. Bose, J. Howard, K.M. Woo, M.J. Edwards and J. Sanz, Phys. Rev. Lett. **114**, 255003 (2015).
12. S.P. Regan et al., Phys, Rev. Lett. **117**, 025001 (2016).
13. L. Ballabio, J. Källne and G. Gorini, Nuclear Fusion **38**, 1723 (1998).
14. T. J. Murphy, Phys. Plasmas **21**, 072701 (2014).
15. B. Appelbe and J. Chittenden, Plasma Phys. Control. Fusion **53**, 045002 (2011).
16. D.H. Munro, J.E. Field, R. Hatarik, J.L. Peterson, E.P. Hartouni, B.K. Spears, and J.D. Kilkenny, Phys. Plasmas **24**, 056301 (2017).
17. M. Gatu Johnson et al., Phys. Rev. E **94**, 021202(R) (2016).
18. V.N. Goncharov et al., Plasma Physics and Controlled Fusion **59**, 014008 (2017).
19. T.R. Boehly, D.L. Brown, R.S. Craxton, R.L. Keck, J.P. Knauer, J.H. Kelly, T.J. Kessler, S.A. Kumpan, S.J. Loucks, S.A. Letzring, F.J. Marshall, R.L. McCrory, S.F.B. Morse, W. Seka, J.M. Soures, and C.P. Verdon, Opt. Commun. **133**, 495 (1997).
20. J.P. Chittenden, B.D. Appelbe, F. Manke, K. McGlinchey, and N.P.L. Niasse, Phys. Plasmas 23, 052708 (2016).
21. See Supplemental material […url...] for a table of target and laser parameters for each individual implosion.
22. S. Skupsky, R.W. Short, T. Kessler, R.S. Craxton, S. Letzring, and J.M. Soures, J. Appl. Phys. **66**, 3456 (1989); S.P. Regan et al., J. Opt. Soc. Am. B **22**, 998 (2005).
23. T.R. Boehly, V.A. Smalyuk, D.D. Meyerhofer, J.P. Knauer, D.K. Bradley, R.S. Craxton, M.J. Guardalben, S. Skupsky and T.J. Kessler, J. Appl. Phys. **85**, 3444 (1999).
24. F.J. Marshall, J.A. Delettrez, R. Epstein, R. Forties, R.L. Keck, J.H. Kelly, P.W. McKenty, S.P. Regan and L.J. Waxer, Phys. Plasmas **11**, 251 (2004).
25. In ICF, the time-scale for burn is short enough where the implosion time can be used as the start signal, and only a single detector is required for the nTOF measurement (the burn duration for these implosions is ~100 ps). Neglecting the impulse response of the detector, $E=0.5m\times d^2/t^2$, where m is the neutron mass, d detector distance, and t flight time.
26. V.Yu. Glebov et al., Rev. Sci. Instrum. **81**, 10D325 (2010); University of Rochester, Laboratory for Laser Energetics, National Laser Users' Facility Users Guide, http://www.lle.rochester.edu/media/about/documents/UsersGuide/05_UsersGuide.pdf (2014).
27. See Supplemental material […url...] for a summary of performance parameters for each individual implosion.
28. J.T. Larsen and S.M. Lane, J. Quant. Spectrosc. Radiat. Transfer **51**, 179 (1994).
29. I.V. Igumenshchev, F.J. Marshall, J.A. Marozas, V.A. Smalyuk, R. Epstein, V.N. Goncharov, T.J.B. Collins, T.C. Sangster, and S. Skupsky, Phys. Plasmas **16**, 082701 (2009).
30. B.M. Haines et al., Phys. Plasmas **23**, 072709 (2016).
31. C. Stoeckl et al., Phys. Plasmas **24**, 056304 (2017).
32. R. Tommasini et al., Phys. Plasmas **22**, 056315 (2015).
33. C.R. Weber et al., Phys. Plasmas **24**, 056302 (2017).
34. A. Pak et al., Phys. Plasmas **24**, 056306 (2017).
35. L. Divol et al., Phys. Plasmas **24**, 056309 (2017).
36. J.R. Rygg, J.A. Frenje, C.K. Li, F.H. Séguin, R.D. Petrasso, F.J. Marshall, J.A. Delettrez, J.P. Knauer, D.D. Meyerhofer, and C. Stoeckl, Phys. Plasmas **15**, 034505 (2008).
37. Offsets of 8-16μm were measured using x-ray pinhole imaging for these implosions.
38. See supplemental material […url...] for a table summarizing the offset measurements.
39. W.R. Donaldson, J. Katz, R. Huff, E.M. Hill, J.H. Kelly, J. Kwiatkowski, R.B. Brannon, and R. Boni, Rev. Sci. Instrum. **87**, 053511 (2016).
40. The beam energy balance is measured prior to entry into the target chamber and must be corrected for transmission through the final optics and blast shields, which can introduce large uncertainties. The implosions described here were taken the day after blast shield replacements, which means the beam energy balance measurements are expected to be accurate.
41. B. Appelbe and J. Chittenden, High Energy Density Physics **11**, 30 (2014). doi:10.1016/j.hedp.2014.01.003
42. D.T. Michel et al., High Power Laser Science and Engineering **3**, e19 (2015). doi:10.1017/hpl.2015.15
43. Wedge Range Filter (WRF) proton spectrometers, Charged Particle Spectrometers (CPS) and the Magnetic Recoil Spectrometer (MRS) were used for these measurements.
44. See the Supplemental material […url...] for a table of inferred ρR values and for references describing the charged-particle spectrometers used to make these measurements.
45. M. Gittings, R. Weaver, M. Clover, T. Betlach, N. Byrne, R. Coker, E. Dendy, R. Hueckstaedt, K. New, W.R. Oakes, D. Ranta and R. Stefan, Comput. Sci. Discovery **1**, 015005 (2008); B.M. Haines, C.H. Aldrich, J.M. Campbell, R.M. Rauenzahn and C.A. Wingate, Phys. Plasmas **24**, 052701 (2017).
46. R.H.H. Scott et al., Phys. Rev. Lett. **110**, 075001 (2013).
47. See Supplemental material […url...] for a table of Chimera-simulated T_{ion}.
48. O.A. Hurricane et al., Nature **506**, 343 (2014).
49. V. Gopalaswamy et al., "Tripling the Fusion Yield in Direct-Drive Laser Fusion through Data-Driven Statistical Modeling", in preparation for submission to Nature (2018).
50. J. L. Peterson, K.D. Humbird, J.E. Field, S.T. Brandon, S.H. Langer, R.C. Nora, B.K. Spears and P.T. Springer, Phys. Plasmas **24**, 032702 (2017).